APPLIED SCIENCES AND ENGINEERING

Wireless smart contact lens for diabetic diagnosis and therapy

Do Hee Keum[1]*, Su-Kyoung Kim[1]*, Jahyun Koo[2]*, Geon-Hui Lee[1], Cheonhoo Jeon[2], Jee Won Mok[3], Beom Ho Mun[4], Keon Jae Lee[4], Ehsan Kamrani[5], Choun-Ki Joo[3], Sangbaie Shin[6], Jae-Yoon Sim[2], David Myung[7,8], Seok Hyun Yun[5], Zhenan Bao[7], Sei Kwang Hahn[1,6,7†]

A smart contact lens can be used as an excellent interface between the human body and an electronic device for wearable healthcare applications. Despite wide investigations of smart contact lenses for diagnostic applications, there has been no report on electrically controlled drug delivery in combination with real-time biometric analysis. Here, we developed smart contact lenses for both continuous glucose monitoring and treatment of diabetic retinopathy. The smart contact lens device, built on a biocompatible polymer, contains ultrathin, flexible electrical circuits and a microcontroller chip for real-time electrochemical biosensing, on-demand controlled drug delivery, wireless power management, and data communication. In diabetic rabbit models, we could measure tear glucose levels to be validated by the conventional invasive blood glucose tests and trigger drugs to be released from reservoirs for treating diabetic retinopathy. Together, we successfully demonstrated the feasibility of smart contact lenses for noninvasive and continuous diabetic diagnosis and diabetic retinopathy therapy.

INTRODUCTION

Recently, soft bioelectronics has been widely investigated to take advantage of its inherent polymer properties and organic electronics for wearable and implantable health care devices (*1*, *2*). On the basis of this innovation, many kinds of medical devices have been developed for diagnostic (*3*), therapeutic (*4*), and theranostic applications (*5*). Wearable devices have been successfully applied in continuous glucose monitoring (*5*), electrocardiography (*6*), electromyography (*7*), photoplethysmography, and pulse oximetry (*8*). They can provide important medical information for health care monitoring and the diagnosis of various relevant diseases. In addition, a pioneering semiconductor implantable drug delivery device was developed for applications in the subcutaneous fluid (*9*) and triggered the development of on-demand implantable drug delivery systems (*10*). Combining these technologies together, many kinds of health care devices have been developed for theranostic applications at the interface of biological, nanoscale, and electronic technologies (*5*, *11*–*13*).

Among various wearable health care devices, smart contact lenses have attracted great commercial attention for health care applications (*14*, *15*). The surface of the cornea uniquely presents a convenient and noninvasive interface to physiological conditions in the human body. The eyes are directly connected to the brain, liver, heart, lung, and kidney and can serve as a window to the body (*16*). In this context, Sensimed released a U.S. Food and Drug Administration (FDA)–approved product, Triggerfish, to monitor the intraocular pressure of glaucoma patients in 2016 (*14*, *15*). In addition, Google developed the Google lens for the diagnosis of diabetic patients in collaboration with Novartis (*15*). These smart contact lenses are especially important because they make noninvasive and continuous monitoring of glaucoma and diabetes, respectively, possible. Furthermore, smart wearable sensor systems integrated on soft contact lenses have been developed to measure the resistance change of graphene sensors upon glucose binding for the remote monitoring of diabetes (*17*, *18*). However, the electrical current and the color changes in the sensors were proportional in log scale to the glucose concentrations, which might not be adequate to measure the real glucose concentration for accurate diabetic diagnosis.

Here, we developed a remotely controllable smart contact lens for noninvasive glucose monitoring and controlled drug delivery to treat diabetic retinopathy. The multifunctional smart contact lens consists of five main parts: a real-time electrochemical biosensor, an on-demand flexible drug delivery system (f-DDS), a resonant inductive wireless energy transfer system, a complementary integrated circuit (IC)–based microcontroller chip with a power management unit (PMU), and a remote radio frequency (RF) communication system (Fig. 1). The real-time amperometric biosensor is designed to detect glucose in tears, replacing the need for invasive blood tests. Drugs can be released from the self-regulated pulsatile f-DDS by remote communication. The resonant inductive coupling to a copper (Cu) receiver coil allows wireless powering from an external power source with a transmitter coil. The device communicates with an external controller by RF communication. We assessed and discussed the feasibility of this smart contact lens for diabetic diagnosis and diabetic retinopathy therapy.

RESULTS

Preparation and characterization of silicone contact lens hydrogels

Silicone contact lens hydrogels were prepared with a chemical structure as schematically shown in fig. S1A. The silicone hydrogels were

[1]Department of Materials Science and Engineering, Pohang University of Science and Technology (POSTECH), 77 Cheongam-ro, Nam-gu, Pohang, Gyeongbuk 37673, Korea. [2]Department of Electrical Engineering, Pohang University of Science and Technology (POSTECH), 77 Cheongam-ro, Nam-gu, Pohang, Gyeongbuk 37673, Korea. [3]Department of Ophthalmology and Visual Science, Seoul St. Mary's Hospital, Collage of Medicine, The Catholic University of Korea, 505, Banpo-dong, Seocho-gu, Seoul 06591, Korea. [4]Department of Materials Science and Engineering, Korea Advanced Institute of Science and Technology (KAIST), 291 Daehak-ro, Yuseong-gu, Daejeon 34141, Korea. [5]Wellman Center for Photomedicine, Massachusetts General Hospital and Harvard Medical School, 65 Landsdowne St., UP-5, Cambridge, MA 02139, USA. [6]PHI BIOMED Co., #613, 12 Gangnam-daero 65-gil, Seocho-gu, Seoul 06612, Korea. [7]Department of Chemical Engineering, Stanford University, 443 Via Ortega, Stanford, CA 94305, USA. [8]Byers Eye Institute at Stanford University School of Medicine, Palo Alto, CA 94304, USA.
*These authors contributed equally to this work.
†Corresponding author. Email: skhanb@postech.ac.kr

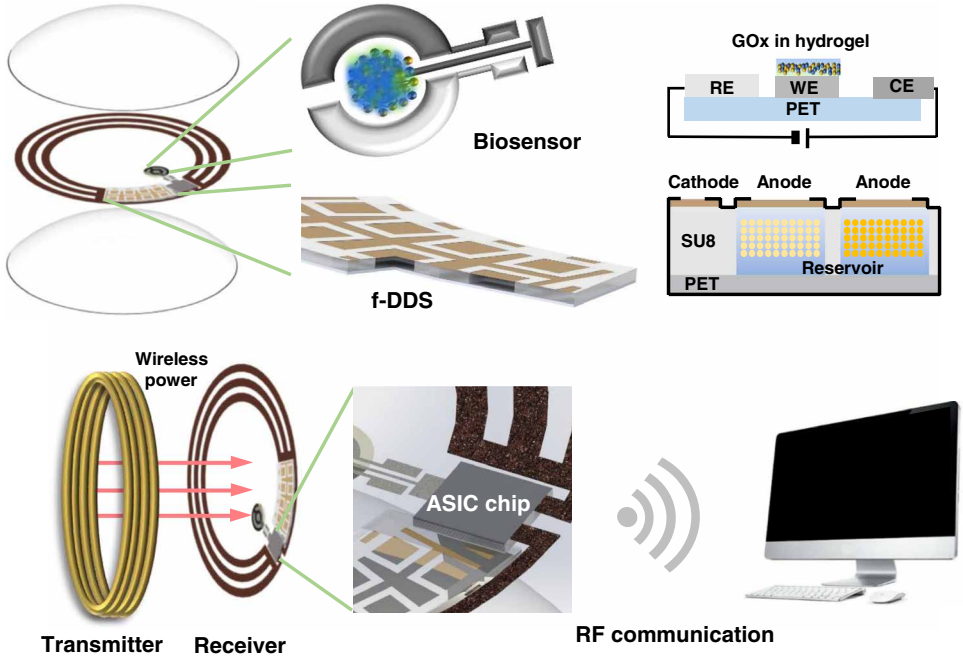

Fig. 1. Schematic illustration of the smart contact lens for diabetic diagnosis and therapy. The smart contact lens is embedded with a biosensor, an f-DDS, a wireless power transmission system from a transmitter coil to a receiver coil, an ASIC chip, and a remote communication system as a ubiquitous platform for various diagnostic and therapeutic applications.

fabricated in the form of a contact lens with a diameter of 14 mm, a thickness of 200 μm, and a radius curvature of 8.0 mm. Attenuated total reflectance–Fourier transform infrared spectroscopy (ATR-FTIR) showed clear peaks corresponding to the chemical attachment of added monomers (fig. S1B). The wavelengths of five peaks were well matched with those of a commercial silicone hydrogel contact lens of lotrafilcon A. The silicone hydrogel contact lens exhibited nearly comparable transmittance to that of the poly(hydroxyethyl methacrylate) (PHEMA) hydrogel contact lens as a control in the visible wavelength range (fig. S1C). The equilibrium water content (EWC) of the silicone hydrogel contact lens was 33.6%, which was higher than those of the PHEMA hydrogel contact lens (21.3%) and lotrafilcon A (24%) (fig. S1D) owing to the high ratio of hydrophilic silicone-containing monomers. The diameter of the silicone hydrogel lens increased by only 1 to 15 mm, whereas that of the PHEMA hydrogel lens increased by 2 to 16 mm. The surface hydrophilicity of the silicone hydrogel contact lens was controlled by the ozone plasma treatment. The surface-treated silicone hydrogel contact lens showed a lower water contact angle than the PHEMA hydrogel contact lens in every time point (fig. S1E), and the water droplet was rapidly absorbed into the silicone hydrogel contact lens (fig. S1F).

In vitro real-time electrical detection of tear glucose concentrations

An ocular glucose sensor was designed with three electrodes to have a low electrical resistance for the facilitated electrochemical glucose reaction (Fig. 2A). The working electrode (WE) and the counter electrode (CE) were prepared with platinum (Pt) for the efficient electrochemical reaction. To enhance the adhesion between polyethylene terephthalate (PET) and Pt, a Cr layer was deposited on the PET substrate as an adhesive layer before Pt layer deposition. The reference electrode (RE) coated with silver/silver chloride (Ag/AgCl) increased the accuracy of amperometric electrochemical glucose sensor in the fluidic environment by providing a constant voltage to the WE during the glucose measurement. To monitor the tear glucose content with high sensitivity and stability, we coated a mixed solution of glucose oxidase (GOx), bovine serum albumin (BSA), poly(vinyl alcohol) (PVA), and chitosan on the WE. After drying, glutaraldehyde was added to cross-link chitosan and PVA for the immobilization of GOx with BSA. To confirm the strong correlation between blood and tear glucose levels, their glucose concentrations in normal and diabetic rabbits were measured before and after three times feeding and fasting. The diabetic rabbits showed higher glucose concentrations both in tear and in blood than those of normal rabbits (Fig. 2B). These blood and tear glucose levels seem to be in the reasonable range, because the normal blood glucose level for nondiabetics while fasting is between 70 and 130 mg dl^{-1} (*19*). Because of the big sampling time interval, we could not observe the lag time in the increase of glucose concentrations between the blood and the tear as reported elsewhere (*19*). However, we made clear the repetitive strong correlation between the blood and the tear glucose levels. These results indicated the feasibility of measuring a tear glucose level as an alternative to the blood glucose measurement for the diagnosis of diabetic diseases.

As shown in Fig. 2C, we could measure the real-time glucose concentration from the electrical current change in vitro using a potentiostat. The current increased from 0.41 to 3.12 μA with increasing glucose concentrations from 5 to 50 mg dl^{-1}. This range of current change might be suitable for the remote monitoring of physiological glucose levels. To assess the selectivity toward glucose, we applied potentially interfering molecules of ascorbic acid (A), lactate (L), and urea (U) in the tear (Fig. 2D). The concentrations of ALU are reported to be around 0.70 mg dl^{-1} for A (*20*), 18 to 45 mg dl^{-1} for L (*21*), and 36 mg dl^{-1} for U (*20*) in the tear. When the corresponding

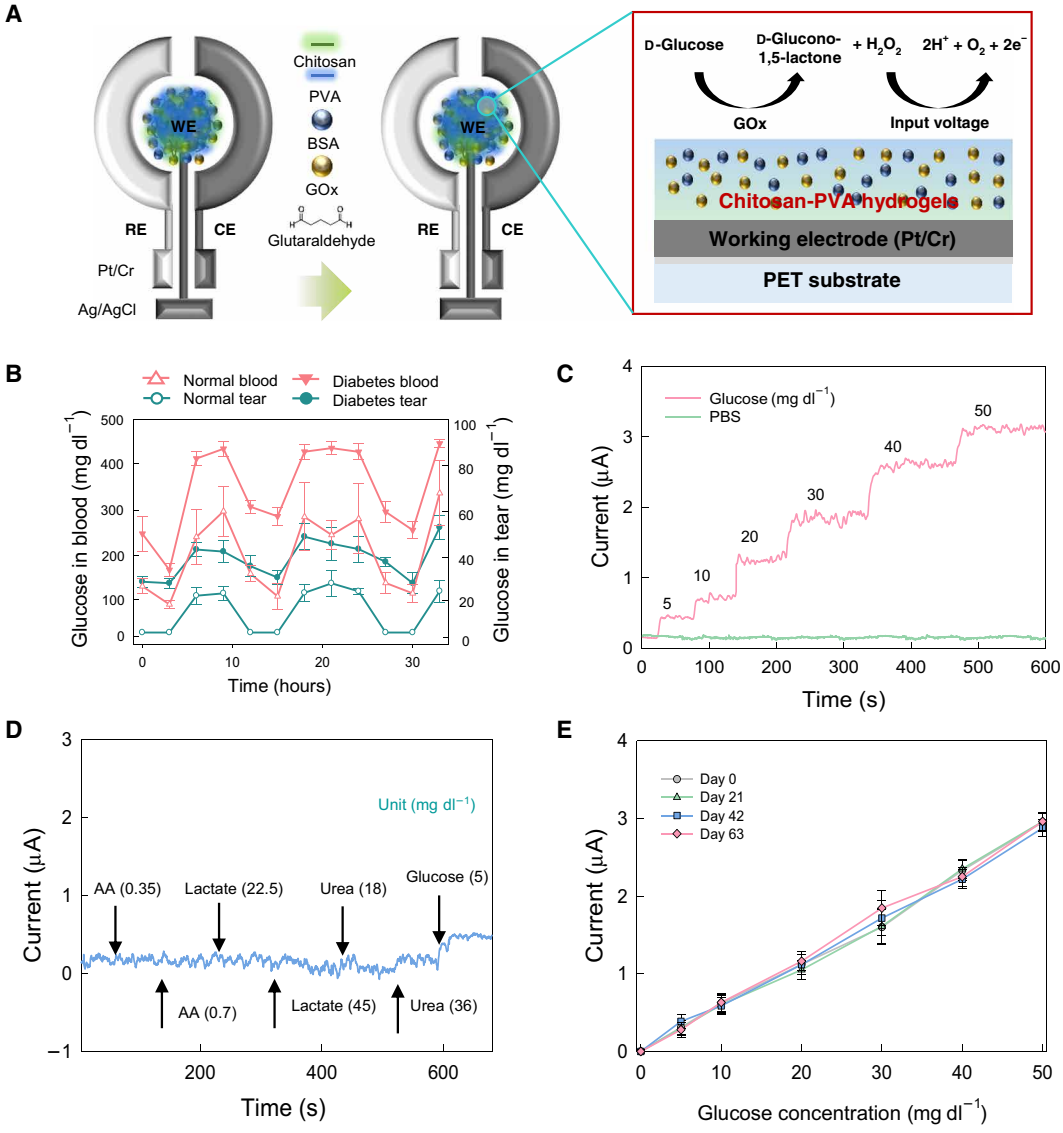

Fig. 2. In vitro electrical detection of ocular glucose sensors. (**A**) Schematic illustration of an ocular glucose sensor with three electrodes (WE, working electrode; RE, reference electrode; CE, counter electrode) and the mechanism of glucose measurement in tear. (**B**) Correlation between blood and tear glucose levels in normal and diabetic rabbit models. (**C**) Real-time electrical detection of glucose concentrations compared with that of PBS. (**D**) Current change of the glucose sensor showing the selectivity to 0.35 and 0.7 mg dl^{-1} ascorbic acid (AA), 22.5 and 45 mg dl^{-1} lactate, 18 and 36 mg dl^{-1} urea, and 5 mg dl^{-1} glucose. (**E**) The long-term stability of the glucose sensor after storage for 0, 21, 42, and 63 days ($n = 3$).

concentrations of interfering molecules (A, L, and U) were added in the glucose sensing system, only a little noise was observed with a negligible current change. Unlike A, L, and U, addition of 5 mg dl^{-1} of glucose rapidly increased the current up to 0.42 μA. In addition, we assessed the long-term stability of glucose sensors (Fig. 2E). After fabrication, smart contact lenses were stored in sterilized phosphate-buffered saline (PBS) at 20° to 25°C, which was similar to the actual contact lens storage environment, for 21, 42, and 63 days. The performance of glucose sensors was maintained stably with less than 2% deviation for up to 63 days ($n = 3$).

On-demand drug release of f-DDS

The f-DDS was fabricated with dimensions of 1.5 mm by 3 mm by 130 μm (Fig. 3, A and B). An exfoliation layer and a buffer silicone oxide (SiO_2) layer were deposited on a glass substrate, and the drug reservoir was covered with a defect-free Au anode electrode. The laser lift-off (LLO) process using an excimer laser locally melted and dissociated the exfoliation layer. A buffer SiO_2 layer supported the upper device layer during the LLO process and blocked the heat flow generated during the laser-induced exfoliation. In addition to controlling the duration time of the laser shot, the thickness of the buffer SiO_2 layer was an important factor for minimizing thermal damage to the device during the LLO process. We used two different photoresists of SU8-5 and SU8-50. SU8-5 has lower viscosity and strength than SU8-50. Accordingly, SU8-5 was used to insulate the electrode except that the drug release site for the stable operation of f-DDS and SU8-50 was used to build the DDS. Cross-sectional scanning electron microscopy (SEM) showed the electrodes and the

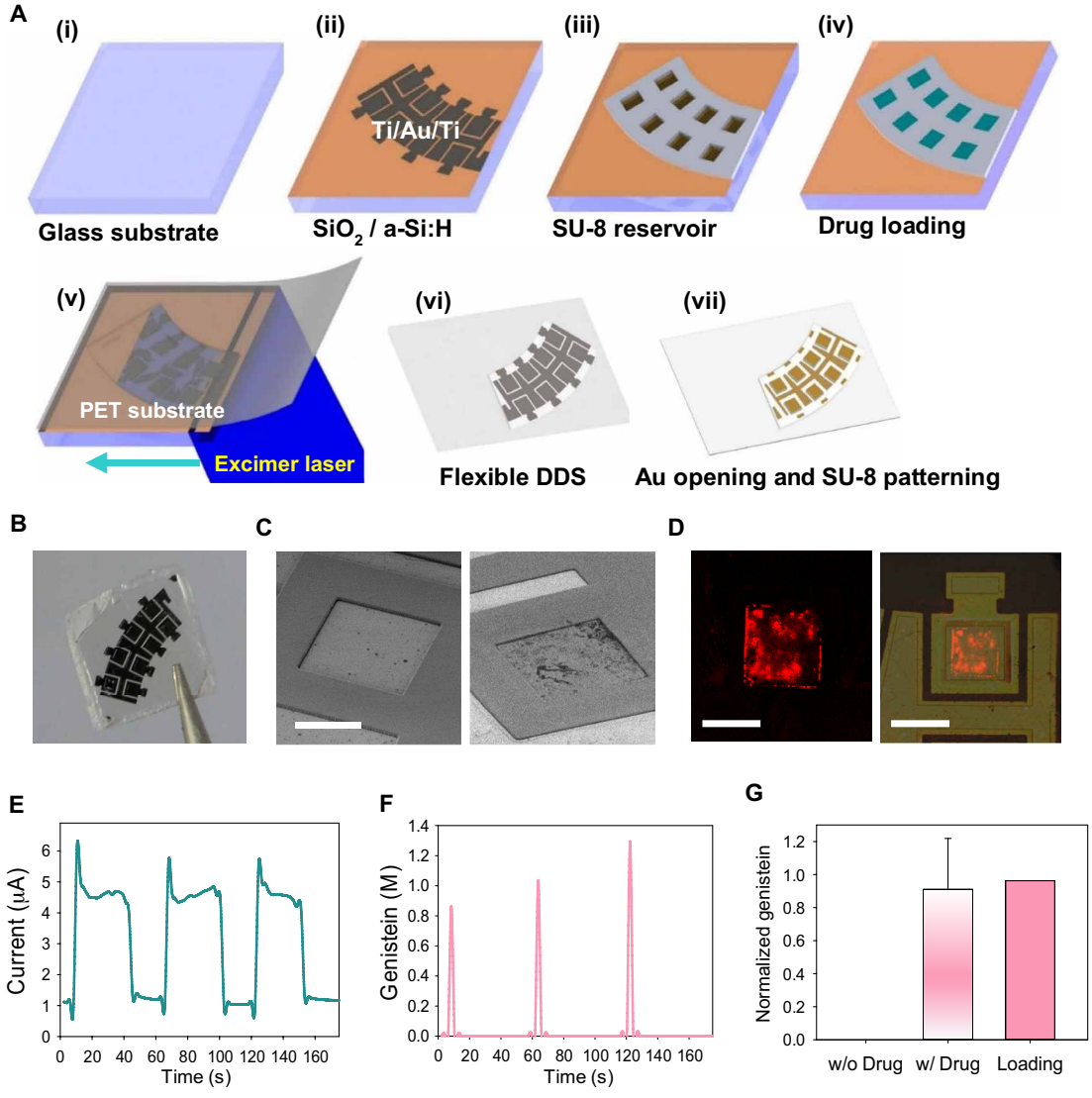

Fig. 3. On-demand drug delivery using an f-DDS. (**A**) Schematic illustration for the fabrication of f-DDS. (i) Growing the buffer silicone dioxide (SiO_2) layer on a glass substrate; (ii) deposition of Ti, Au, and Ti metals for anode and cathode electrodes; (iii) patterning SU8 drug reservoirs; (iv) drug loading; (v) attaching PET and laser scanning of the device; (vi) detaching f-DDS; and (vii) Ti etching with SU8 insulation. (**B**) Photograph of f-DDS. Photo credit: Beom Ho Mun, KAIST. (**C**) SEM images of f-DDS before and after gold electrochemistry test. Scale bar, 250 μm. (**D**) Confocal fluorescence microscopic images of rhodamine B dye released from drug reservoirs. Scale bars, 300 μm (left) and 500 μm (right). (**E**) Current change of the f-DDS. (**F**) Released concentration of genistein in a pulsatile manner. (**G**) Normalized content of genistein released from the reservoirs ($n = 6$) in comparison with the initial loading content.

insulated layers of the reservoir (fig. S2). The mechanical bending test was performed to evaluate the mechanical reliability of f-DDS on a flexible substrate (fig. S3, A and B). The operating current of f-DDS was maintained without any notable changes during the mechanical durability test up to 1000 cycles (fig. S3C).

The loaded drugs were selectively released from the drug reservoir by the on/off control of voltage. As shown on the SEM image of the Au anode electrode, a thin Au membrane covered the whole area of drug-loaded reservoirs without any leakage of drugs (Fig. 3C, left). After applying an electrical voltage of 1.8 V, the Au membrane was dissolved within 40 s (Fig. 3C, right). The Au layer was melted in PBS under constant voltage in the form of $AuCl_4^-$. Confocal fluorescence microscopy showed the red rhodamine dye released from a reservoir by applying the electrical potential (Fig. 3D). The current between anode and cathode electrodes increased up to 6.08 ± 0.16 μA, and Au anodes were slowly dissolved under a slight current decrease from 6.08 ± 0.16 μA to 4.35 ± 0.11 μA (Fig. 3E). Genistein was released in a pulsatile manner from three different drug reservoirs (Fig. 3F). The anode was slowly dissolved by the current in microscale, and the drug was almost completely released after the current was recovered to the initial state. We could detect 89.97 ± 37.10% of loaded genistein in PBS, confirming that a therapeutic amount of drug might be released from f-DDS (Fig. 3G). In addition, a diabetic therapeutic amount of metformin could be released from the smart contact lens by the synchronized feedback for the point-of-care therapy and further theranostic applications (fig. S3D).

Wireless power transmission and remote communication

A wireless power transmission system was developed via resonant inductive coupling. The receiver coil embedded in the smart contact

lens received a different electrical power from the transmitter coil depending on the distance (fig. S4A). The efficiency of wireless power transmission between two coils was measured with a network analyzer, which was inversely proportional to the distance (fig. S4A). The required power consumption of PMU, the sensor readout block, and the remote communication unit (RCU) on the smart contact lens was 43, 34.4, and 2.3 mW, respectively (fig. S4B). The RCU transmitted data at a rate of 445 kbits·s^{-1} in the 433-MHz industry-science-medical (ISM) frequency band using on-off keying modulation and could be controlled to turn off for power saving when data were not transmitted. Using resonant inductive coupling, the application-specific integrated circuit (ASIC) chip connected to an additional capacitor for energy storage successfully received electromagnetic power at a 1-cm distance from the transmitter coil with an efficiency of 2%. The efficiency was sufficient to maintain the basic operation and the remote communication of the smart contact lens. The average output code of the analog-to-digital converter (ADC) from the ASIC chip was proportional to the input current (fig. S5, A and B). The total input conversion was available up to 4.1 μA with a resolvable input of 150 pA, which was suitable for the electrical detection of glucose using the ocular glucose sensor. The ocular glucose sensor and the f-DDS were operated under the control of the ASIC chip by applying the corresponding bias voltages (fig. S5, B and C). The converted data of the biosensor were serialized by the ASIC chip and successfully transmitted to an external device of the personal computer (PC) using the wireless power and remote communication systems (fig. S5D).

Fabrication and assessment of the integrated smart contact lens

On the basis of preliminary experimental results, a smart contact lens was fabricated by the chemical cross-linking of silicone hydrogel precursor solution containing a PET film, which was embedded with a glucose biosensor, an f-DDS, an ASIC chip, a Cu power receiver, and RF communication coils and passivated with Parylene C (fig. S6A). The reader coil, which was connected to a commercial power amplifier, wirelessly transferred enough electrical power to the smart contact lens for the real-time sensing of glucose in tear and the remote control of f-DDS (fig. S6B). A constant potential was applied on the RE of the electrochemical glucose sensor, enabling high sensitivity and stability. The output data of the biosensor were wirelessly transmitted by the remote communication using a custom-made amplitude shift keying (ASK) receiver module, an Alf Vergard Risc (AVR), and a PC. The remotely transferred data showed that the current change of glucose sensor was proportional to the applied glucose level in vitro, confirming the feasibility for real-time wireless electrical glucose detection using the smart contact lens (fig. S6C). The output current change values of 0.40 to 3.13 μA were similar to those of the glucose measurement using a potentiostat in vitro in Fig. 2C. In addition, on-demand drug delivery was demonstrated by the remote control of the ASIC chip to apply a constant voltage of 1.8 V to the f-DDS (fig. S6C). The silicone hydrogel contact lens with a high water content did not cause any substantial damage to the biosensor, f-DDS, and other micro-sized components.

In vivo diagnostic and therapeutic applications of the smart contact lens

Before in vivo applications, the safety of the integrated smart contact lens was evaluated in the eyes of New Zealand white rabbits for a period of 5 days (fig. S7). Histological analysis of extracted rabbits' eyes with hematoxylin and eosin (H&E) staining did not show any notable damage on the corneal epithelia, stroma, and endothelia of rabbits after wearing smart contact lenses for 3 and 5 days in comparison with the normal cornea of rabbits. Although our smart contact lens induced some degree of corneal swelling, it did not incite an inflammatory reaction after 5 days. The corneal swelling was likely caused by the poor oxygen transfer through the closed eyelid during sleep while wearing the contact lens, which leads to the accumulation of lactic acid and water inside the cornea as a result of osmotic shift. No infections or serious adverse ocular surface reactions or changes were observed with the lens in place. Overall, our results demonstrated the preliminary safety of the smart contact lens while placed on the eye.

After that, we carried out the assessment of the integrated smart contact lens on diabetic rabbit eyes for biosensing and drug delivery applications as schematically shown in Fig. 4A. The integrated wireless smart contact lens for glucose sensing only (fig. S8A) or that for both glucose sensing and drug delivery (fig. S8B) was worn on the rabbit eye and operated by wireless power transfer between an external transmitter coil and a receiver coil on the smart contact lens (fig. S8C). The portable power transmission system can be ultimately installed on smart glasses or smart phones as schematically shown in Fig. 4A. Diabetic rabbits were injected with insulin, anesthetized with ketamine, and fitted with our smart contact lens (movie S1). After wearing the smart contact lens, the ocular glucose sensor indicated the increase of glucose concentration up to 30.53 mg dl^{-1} by contacting the tear glucose and then the decrease down to 16.72 mg dl^{-1} by the insulin effect on the glucose metabolism, which was well matched with the blood glucose concentration profile determined by a glucometer (Fig. 4B). The real tear glucose level measured by glucose assay was well matched with the converted glucose level from the output current values. Parviz's group previously developed a contact lens sensor system and performed wireless glucose monitoring using a polydimethylsiloxane (PDMS) eye model (*20*, *22*). While the online sensor output current was in the range of 0 to 400 nA for the glucose concentration of 0 to 10.81 mg dl^{-1} (*20*), the wireless sensor output current was in the range of 0 to 80 nA for the glucose concentration of 0 to 36.03 mg dl^{-1} (*22*). In contrast, we wirelessly measure the real tear glucose level in a wide physiologically meaningful range of 0 to 49.9 mg dl^{-1} in vitro and in vivo with the improved sensitivity (Figs. 2C and 4B and fig. S6C).

Furthermore, we could remotely trigger the release of antiangiogenic genistein from f-DDS on the smart contact lens by applying the electrical potential on-demand. Figure 4C shows the fluorescence microscopic images of cryo-sectioned cornea, sclera, and retina. The genistein released from the smart contact lens appeared to be effectively delivered through the cornea to the retina. The weak fluorescence in sclera revealed that genistein had passed through the sclera with little absorption. In the case of the control, no fluorescence was observed in the cryo-sectioned tissues of rabbits wearing the smart contact lens without genistein or the smart contact lens with genistein without electrical triggering for its release (Fig. 4C, below). From the results, we could confirm the feasibility of the smart contact lens for electrically controlled on-demand ocular therapeutic drug delivery (Table 1).

An infrared thermal camera showed no notable temperature change in the body of the smart contact lens on rabbit eyes (Fig. 4D). In the beginning, the temperature of the smart contact lens was 32.4°C, that of the ocular surface was 34.4°C, and that of the external coil

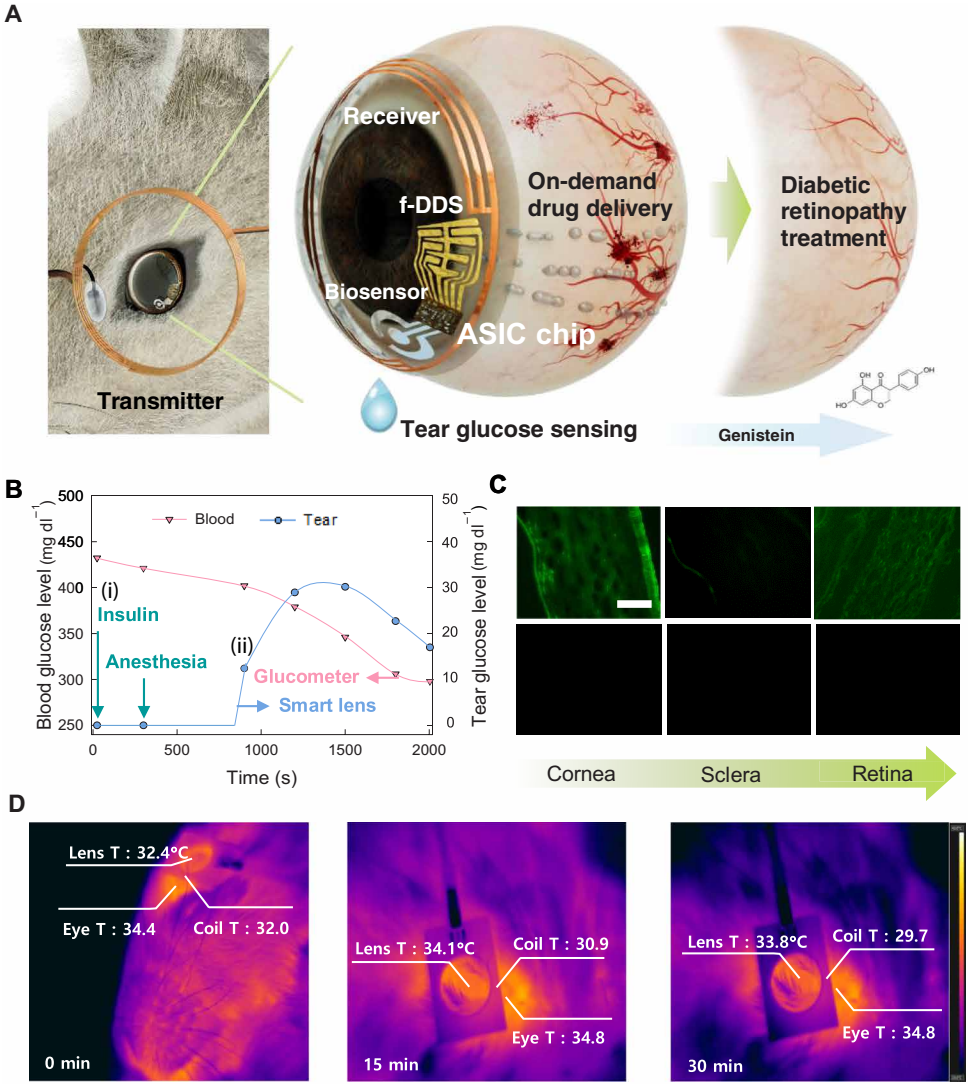

Fig. 4. In vivo applications of smart contact lens systems. (**A**) Schematic illustration for in vivo diabetic diagnosis and therapy of the smart contact lens. (**B**) In vivo real-time wireless measurement of tear glucose levels with the smart contact lens. The blood and tear glucose levels were measured (i) after injection of insulin and anesthesia for wearing the smart contact lens in PBS. (ii) The tear glucose level increased due to the glucose in tears and decreased, reflecting the blood glucose level decrease due to the injected insulin. The blood glucose level was measured every 5 min with a commercial glucometer. (**C**) Fluorescence microscopic images of drugs absorbed in cornea, sclera, and retina of rabbits wearing the smart contact lens loaded with (top row) and without (bottom row) genistein. Scale bar, 0.1 mm. (**D**) Infrared thermal camera analysis for the temperature of the eye, smart contact lens, and transmitting coil after operating for 0, 15, and 30 min.

was 32.0°C. After 30 min of operation, the temperature of the smart contact lens was 33.8°C with a temperature increase of 1.4°C, that of the ocular surface was 34.8°C with a temperature increase of 0.4°C, and that of the external coil was 29.7°C with a temperature decrease of 2.3°C. The slight temperature increase revealed the thermal safety of our smart contact lens.

Therapeutic effect of genistein released from the smart contact lens on diabetic retinopathy

New Zealand white rabbits were divided into five groups to assess the therapeutic effect of genistein released from the smart contact lens on diabetic retinopathy compared to a series of control and comparator groups. The left eyes of rabbits were treated with a topical eye drop of PBS as a negative control in group 1, a topical eye drop of genistein in group 2, intravitreal injection of genistein in group 3, and intravitreal injection of Avastin as a positive control in group 4. The right eyes of all groups were treated with smart contact lenses containing genistein (which collectively comprised group 5). Transmission electron microscopy (TEM) visualized the inhibitory effect of genistein released from the smart contact lens on the deformation of retinal vascular structure (Fig. 5A). The diabetic retinal vessels in Fig. 5A(iv) (left eye of group 4) and Fig. 5A(v) had a round shape surrounded by the thick vascular endothelial cell (EC) layers, which were comparable to that of the healthy rabbit (*23*). However, the vascular basement membrane appeared to be irregular and folded without the clear vascular EC layer in Fig. 5A(i) (left eye of group 1), reflecting increased vascular permeability and the blood-retinal barrier breakdown. In Fig. 5A(ii) (left eye of group 2) and Fig. 5A(iii) (left eye of group 3), the vessels had a round shape, but the surrounding vascular EC layers were not as thick as those in Fig. 5A(iv and v).

Table 1. Comparison of various smart contact lenses.

Smart contact lens types	Biosensing	Glucose sensing range	Therapy	Power system	Data transfer	Current status
Triggerfish (*14*)	Intraocular pressure	×	×	Inductive coupling	RF communication	FDA-approved
Google lens (*15*)	Glucose	0 ~ 36 mg dl^{-1}	×	Inductive coupling and Li battery	Reflectance from inductive coupling	Clinical
The Park group contact lens (*17*, *18*)	Intraocular pressure and glucose	0 ~ 180 mg dl^{-1} (log scale dependence)	×	Inductive coupling	Reflectance from inductive coupling	*In vivo*
The Parviz group contact lens (*20*, *22*)	Glucose	0 ~ 36 mg dl^{-1}	×	Online power, RF power	Line connection, backscatter communication	*In vitro*
Our smart contact lens	Glucose	0 ~ 50 mg dl^{-1}	Drug delivery	Inductive coupling	RF communication	*In vivo*

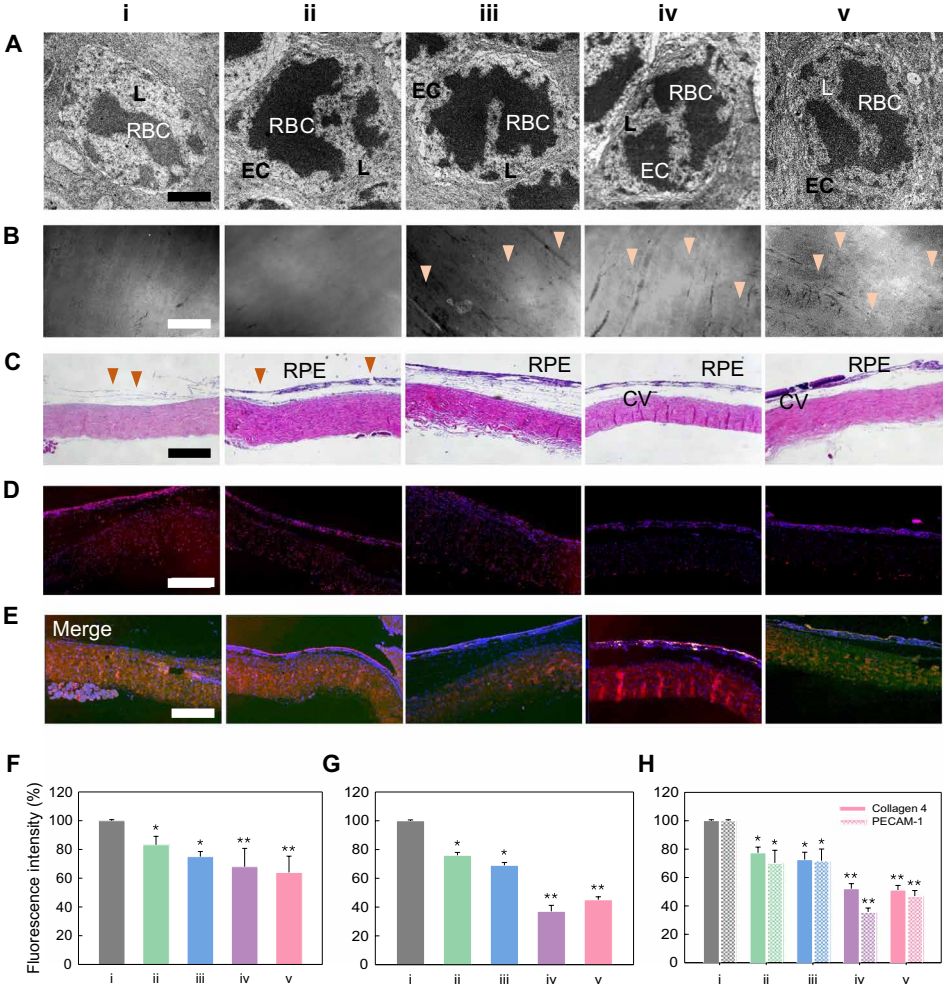

Fig. 5. In vivo therapeutic effect of genistein released from the smart contact lens. The eyes of diabetic rabbits were treated with (i) an eye drop of PBS (control), (ii) an eye drop of genistein, (iii) intravitreal injection of genistein, (iv) intravitreal injection of Avastin, and (v) genistein released from the smart contact lens. (**A**) Electron micrographs of the retinal vessels. L, lumen of vessel; EC, endothelial cell; RBC, red blood cell. Scale bar, 1 μm. (**B**) Fluorescence angiograms of the retina (arrowheads, retinal vessels). Scale bar, 0.2 mm. (**C**) Histological analysis for the damage to the retinal pigment epithelium (RPE) and choroidal vessels (CVs) (arrowheads, damage in CV). Scale bar, 0.1 mm. (**D**) Apoptosis detection in retina by TUNEL assay. Scale bar, 0.1 mm. (**E**) Merged images of immunohistochemistry staining for collagen type 4 (red) and PECAM-1 (green) with nuclear staining by 4′,6-diamidino-2-phenylindole (blue). Scale bar, 0.1 mm. (**F**) Fluorescence intensity of retinal choroidal neovascularization lesion quantified from the images of (B). (**G**) Fluorescence intensity of TUNEL assay quantified from the images of (D). (**H**) Immunochemical fluorescence intensity (E) of collagen type 4 (filled box) quantified from the images in fig. S9A (red) and PECAM-1 (dashed box) quantified from the images in fig. S9B (green) [$n = 3$, $^{*}P < 0.05$ and $^{**}P < 0.01$ versus the control sample of (i)].

Figure 5B shows fluorescence angiograms for the morphology of retinal vessels. While no clear morphology of vessels was observed in Fig. 5B(i and ii), retinal vessels (arrowheads) with clear morphology were observed with the notably decreased retinal vascular permeability in Fig. 5B(iv and v). Fluorescence was observed throughout the retinal parenchyma owing to the increased vascular leakage after blood-retinal barrier breakdown, as quantified in Fig. 5F. In Fig. 5B(iii), little fluorescence was observed with only a scant vasculature. The results of histological H&E analysis were consistent with those of TEM images and fluorescence angiograms (Fig. 5C). In addition, retinal cell death was validated by terminal deoxynucleotidyl transferase–mediated deoxyuridine triphosphate nick end labeling (TUNEL) assay in retinal cross-sectioned images (Fig. 5D). Fluorescence of TUNEL assay was quantified by ImageJ program. When the mean fluorescence intensity in Fig. 5D(i) was set to be 100%, the mean percentage of fluorescence intensity was 76.0% in Fig. 5D(ii), 69.0% in Fig. 5D(iii), 37.0% in Fig. 5D(iv), and 45.1% in Fig. 5D(v) (Fig. 5G). Furthermore, the immunohistochemical staining for collagen type 4 and platelet EC adhesion molecule–1 (PECAM-1) revealed the therapeutic effect of genistein released from the smart contact lens (Fig. 5E). The expression degree of collagen type 4 and PECAM-1 was lower in fig. S9(iv and v) than in fig. S9(i to iii) (Fig. 5H).

DISCUSSION

Smart electronic contact lens devices have been widely investigated for diagnostic applications, especially for continuous glucose monitoring and intraocular pressure monitoring. In addition, there have been many reports on the electrical and optical glucose sensing with improved sensitivity using various nanomaterials (*24*–*26*). To improve the sensitivity, stability, and reproducibility, we immobilized GOx in the chitosan and PVA hydrogels together with BSA. PVA appeared to mitigate the problem of uneven coating and cracking by increasing the viscosity of the GOx mixture solution with the increased loss modulus (*27*). PVA was also reported to have a substantial effect on the sensitivity of glucose sensors (*28*, *29*). As shown in Fig. 2, the glucose concentrations could be accurately measured from the electrical current change using our glucose sensor, showing the stability for the repeated glucose sensing even after storage for more than 63 days (Fig. 2E) and enabling the real-time continuous tear glucose monitoring in live rabbit eyes in comparison with the blood glucose sensing by a glucometer (Fig. 4B). In contrast, Parviz's group used a model eye and Park's group dropped glucose samples directly onto the rabbit eyes after wearing the smart contact lens for the assessment of their electrochemical glucose sensors, and there is no scientific journal report on in vivo glucose sensing of the Google lens (Table 1).

Despite the intensive effort for the commercial development of Google lens, they recently reported that there was insufficient consistency in their measurements of the correlation between tear glucose and blood glucose concentrations to support the requirements of a medical device. The disappointing clinical results might be associated with the challenges of obtaining reliable tear glucose readings in the complex on-eye environment. Although the correlation between tear and blood glucose concentrations remains controversial, there are many reports supporting the strong correlation between them (*15*, *17*–*19*). As shown in Fig. 4B, we could perform real-time continuous tear glucose monitoring in live rabbit eyes, which was strongly correlated with the blood glucose concentrations. We believe that with proper calibration and baseline monitoring, the changes in glucose concentrations can be measured reliably for each patient using the smart contact lens. This is similar to that of the FDA-approved Triggerfish lens that measures changes in intraocular pressure rather than an absolute intraocular pressure.

On top of that, our smart contact lens has a unique function of ocular drug delivery. To date, a variety of drug-eluting contact lenses have been developed using biodegradable polymer nanoparticles and micelles to improve the efficiency of ocular drug delivery. However, there has been no report on smart contact lenses with an electrically controlled on-demand DDS, possibly due to the difficulty in the miniaturization of all these electronic components onto the small contact lens. Antiangiogenic genistein and the glucose level–controlling metformin could be delivered from the f-DDS on the smart contact lens (Figs. 3 and 4 and fig. S3). The released genistein could be delivered through the cornea to the retina as shown in Fig. 4, exhibiting the therapeutic effect on diabetic retinopathy. This smart contact lens for wireless biosensing and therapeutic drug delivery might pave a new avenue to ubiquitous health care for further theranostic applications. Although metformin has been commercialized as an oral drug, its therapeutic effects through various other delivery routes have been well documented, such as transdermal delivery (*25*) and ocular delivery (*30*, *31*). Berstein (*31*) reported that metformin is not simply an oral drug and that it influences many reactions and processes such as proliferation, apoptosis, angiogenesis, and oxidative stress in cell lines and, given these findings, stated that it is very reasonable to target metformin for topical and ocular delivery applications.

Concerning the safety issue of the smart contact lens, the wireless energy transfer system should be carefully investigated because of the possible ocular damage by the generated heat of the smart contact lens. In this context, we measured the heat from operating the contact lens using an infrared thermal camera, which showed no notable temperature change in the smart contact lens on rabbit eyes (Fig. 4D). The only slight temperature increase revealed the thermal safety of our smart contact lens. Optical images and histological analyses of corneas in the eyes of New Zealand white rabbits also confirmed the safety of our smart contact lens (fig. S7). From all these results, we could confirm the preliminary safety of our smart contact lens for further applications. Moreover, the FDA approval for the clinical use of Triggerfish is an important supporting information on the safety of smart contact lenses.

In summary, a smart electrochemical contact lens has been successfully developed with a glucose biosensor and an f-DDS controlled by wireless power and remote communication systems for both diabetic diagnosis and therapy. We demonstrated the real-time biosensing of glucose concentrations in the tear and on-demand therapeutic drug delivery of genistein for the treatment of diabetic retinopathy in diabetic rabbit eyes. The ocular glucose biosensor uniformly coated with GOx immobilized in the cross-linked hydrogels of chitosan and PVA with BSA showed high sensitivity, linearity, and stability for the repeated applications after long-time storage for 63 days. The genistein delivered from the smart contact lens through the cornea to the retina showed a comparable therapeutic effect to that by the intravitreal injection of Avastin on diabetic retinopathy. This smart theranostic contact lens will be investigated further as a next-generation wearable device to achieve the real-time biosensing of ocular biomarkers and on-demand medication for ubiquitous health care applications to various ocular and other diseases.

MATERIALS AND METHODS

Preparation of contact lens materials

Silicone contact lens hydrogels were prepared under nitrogen by the photocrosslinking of 2-hydroethylmethacrylate (HEMA), silicone-containing monomers of 3-(trimethoxysilyl)propyl methacrylate, 3-[tris(trimethylsiloxy)silyl]propyl methacrylate, and a cross-linker of ethyleneglycol dimethacrylate (EGDMA) for 15 min using a photoinitiator of Darocur TPO, diphenyl(2,4,6-trimethylbenzoyl)phosphine oxide. As a control, PHEMA contact lens hydrogels were prepared by mixing HEMA and EGDMA with the photoinitiator. To form a contact lens shape, the precursor solution was loaded on a polypyrrole mold under ultraviolet (UV) light at a wavelength of 254 nm for 8 min. Silicone and PHEMA hydrogel contact lenses were detached from the mold and surface-treated under oxygen plasma (OptiGlow ACE, Glow Research). The prepared contact lens was completely submerged in PBS at 37°C for a day before use.

Characterization of contact lens materials

ATR-FTIR (Tensor 27, Bruker) of dehydrated silicone hydrogel contact lens and lotrafilcon A was recorded over the 400 to 4000 cm^{-1} range. The transmittance of silicone and PHEMA hydrogel contact lenses was measured using a UV-visible spectrometer (SD-1000, Scinco) after soaking in PBS for 24 hours. Both samples were placed in quartz plates, and the transmittance was measured at the wavelength range of 250 to 1000 nm. The EWC was determined by weighing the dried contact lens (W_{dry}) and the hydrated contact lens with soaking in PBS for 24 hours (W_{wet}). The value of EWC was calculated as the percentage of the weight gain during hydration and dehydration using the following equation: $EWC = (W_{wet} - W_{dry})/W_{dry} \times 100$ (*32*). The water contact angles on dried silicone and PHEMA contact lenses were measured in static mode by dropping 5 μl of water every 2 min (SmartDrop, FemtoFAB).

Fabrication of ocular glucose sensor

Three WE, CE, and RE in the glucose sensor were patterned with 20-nm-thick chromium (Cr) and 80-nm-thick Pt on a 0.23-μm-thick PET substrate using an electron beam evaporator. RE was additionally treated to form a 200-nm-thick silver (Ag) layer. For the long-term stability, all parts of the glucose sensor except WE, CE, and RE were passivated with Parylene C. For chlorination, the Ag layer was dipped in $FeCl_3$ (1 M, Sigma-Aldrich) solution for 1 min. Then, PVA [2 weight % (wt %), 100,000 g mol^{-1}, Sigma-Aldrich] was dissolved in deionized water and chitosan (0.5 wt %, mid molecular weight, Sigma-Aldrich) was dissolved in acetic acid (1 M, Sigma-Aldrich) with vigorous stirring at 80°C for 12 hours. BSA (10 mg ml^{-1}, Sigma-Aldrich) and GOx (50 mg ml^{-1}, Sigma-Aldrich) were dissolved in 2 wt % of PVA solution, which was mixed with the chitosan solution. The mixed solution was stored in a desiccator to remove bubbles. To uniformly fabricate a GOx layer only on the WE, all areas of the sensor except WE were passivated with PDMS. Then, glucose sensors were treated with UV in the presence of ozone for 10 min. After removing PDMS, 1.8 μl of the prepared GOx mixture solution was dropped onto WE and dried in a desiccator. Last, 1.8 μl of glutaraldehyde (2 wt %, Sigma-Aldrich) was dropped on the GOx layer and dried slowly at 4°C.

In vitro electrical detection of glucose

In vitro electrical glucose measurements were conducted using a potentiostat (Ivium Tech. Co., AJ Eindhoven, The Netherlands) and a computer-controlled ADC (6030E, National Instruments). A 50-ml beaker was filled with 10 ml of PBS (1 M, pH 7.4). The glucose sensor was put into the beaker to dip the sensing area sufficiently in PBS. The glucose sensor detected the change of electrical current under a constant potential of 0.7 V versus Ag/AgCl for steady-state amperometric current responses. After stabilizing the glucose sensor, a high concentration of glucose solution (10,000 mg dl^{-1}, Wako) was added in PBS to slowly change the glucose concentration in the beaker from 5 to 50 mg dl^{-1}, and the change of current was monitored for the glucose quantification. To investigate the selectivity and specificity of the glucose sensor, the change of current was measured after adding the potentially interfering molecules such as A (0.1 M, Sigma-Aldrich), L (10 M, Sigma-Aldrich), and U (10 M, Sigma-Aldrich) in PBS. The long-term storage stability and the repeated usability of the glucose sensor were assessed at days 0, 21, 42, and 63 after fabricating the glucose sensors. The glucose sensors were stored at 20° to 25°C in 5 ml of sterilized PBS (1 M, pH 7.4), similar to the conventional contact lens storage condition.

Fabrication and characterization of f-DDS

On-demand f-DDS was prepared by the LLO process. First, hydrogenated amorphous silicon (a-Si:H) exfoliation and SiO_2 buffer layers were grown by plasma-enhanced chemical vapor deposition. Anode and cathode electrodes of the f-DDS were covered with 10-nm-thick Ti, 80-nm-thick Au, and 10-nm-thick Ti by e-beam evaporation and lithography. The reservoirs were patterned with 100-μm-thick negative photoresists (SU8-5 and SU8-50) with dimensions of 500 μm by 500 μm. As a model drug, 25 nl of genistein (3 M, Sigma-Aldrich) or metformin (2 M) with rhodamine B (Sigma-Aldrich) dye was loaded in the reservoirs. Subsequently, drug-loaded reservoirs were sealed with a flexible PET film. The XeCl excimer laser was exposed on the back side of the glass substrate to separate the SU-8 drug reservoir on the PET film from the glass substrate. For the mechanical bending test, the entire f-DDS was bent with a bending radius in the range of 5 to 30 mm and the electrical current was measured with a probe station. The durability of the f-DDS was assessed by applying 1000 bending cycles at a fixed bending radius of 5 mm.

Characterization of f-DDS

The drug release in response to applied voltage was investigated by connecting anode and cathode electrodes with the probe station. The constant electrical potential of 1.8 V was applied between anode and cathode electrodes for 1 min. Rhodamine dye released from the reservoir was visualized by confocal microscopy (Leica) using the corresponding imaging software (FluoView). The excitation wavelength was 543 nm and the emission wavelength was in the range of 560 to 610 nm. The concentration of released genistein and metformin in PBS was quantified with a spectrofluorometer (Thermo Fisher Scientific) at excitation/emission wavelengths of 355/460 nm and 485/538 nm, respectively.

Fabrication of power transmission coils

To fit into a contact lens, a wireless power receiver composed of a copper (Cu) coil was prepared with a thickness of 0.1 mm and an outer diameter of 1.2 mm. PDMS was spin-coated on a glass substrate, attaching 0.1 mm of Cu foil (Sigma-Aldrich). After polymerization of PDMS in an oven at 70°C for 1 hour, the Cu foil was patterned by photolithography. The foil was wet-etched in 5 ml of ammonium persulfate solution (12 mg ml^{-1}) for 6 hours and detached from the PDMS. Then, the Cu coil was rinsed with acetone, ethanol, and

distilled water for 10 min with sonication, respectively. The power transmitting coil was fabricated using four-turned Cu wire (Sigma-Aldrich) with a thickness of 1 mm and an outer diameter of 5 cm.

Power transmission efficiency measurement

The wireless power transmission system consisted of a Cu power transmitter coil, a Cu power receiver coil in a contact lens, a function generator (AFG 3101, Tektronix), a commercial power amplifier module (MAX 7060), and an ASIC chip. The power amplifier module was used to supply sufficient power to the ASIC chip. The transmitter coil transferred the power to the receiver coil by resonant inductive coupling. The receiver coil embedded in the contact lens was aligned in parallel to the transmitter coil with a distance from 0 to 4 cm to measure its efficiency. The efficiency of wireless power transmission between two coils was measured by using a network analyzer (N5230A, Agilent).

Design and fabrication of the ASIC chip

The ASIC chip is custom-built by multiwafer process fabrication. The ASIC chip was fabricated by Taiwan Semiconductor Manufacturing Company using a 180-nm complementary metal-oxide semiconductor (CMOS) process. The PMU rectified incoming alternating current (ac) energy from the coil to direct current (dc) supply voltage and generated various regulated voltages for other subunits. An RCU transmitted data through 433-MHz on-off keying modulation. A reference clock generator (CLK_{REF}) was implemented with a relaxation oscillator for the system timing. A potentiostat with three nodes (WE, RE, and CE) was integrated into the ASIC chip by Au flip-chip bonding. The potentiostat applied a voltage bias of 1.2 V on the RE and 1.85 V on the WE using an operational amplifier with negative feedback. The change of electrical current was monitored in real time by dropping the glucose sample solution. An integrated ADC received the current input from the potentiostat and converted it to a 15-bit digital output code (*33*). The output codes were then externally transmitted through the ISM frequency band of 433 MHz using the RCU. The current sensing performance of ΔΣ ADC was measured by applying current input from a current supplier (B2961A, Agilent). To suppress the effect of large noise from the equipment, software-based filtering was applied to the measured digital codes. The RF receiver module passed the received data to the AVR, and the AVR communicated with a PC using an RS-232 protocol. The software decoded the data packets and displayed the raw data to the PC.

Power management of the ASIC chip

The PMU wirelessly received AC power and converted it into DC with a MOS-based rectifier, generating the external rectified voltage (V_{EXT}). A bandgap reference circuit generated a reference voltage of 1.2 V, which was up-converted to 1.85 V and buffered with a regulator to provide an internal supply voltage (V_{INT}), driving overall control logic blocks of the ASIC chip. For controlled drug delivery, anode and cathode electrodes in the f-DDS were connected to the PMU that selectively operated the f-DDS according to control commands received from the external reader.

Remote communication system

The RCU consisted of a 433-MHz tuned inductor-capacitor (LC) transmitter and its control logics. Control logics serialized the ADC output and patched a predefined header to define the packet boundary. The carrier frequency was determined by internal capacitors with an external loop antenna (L). Data modulation was performed by controlling the impedance change of the LC transmitter that could be observed by the external reader. An ASK receiver in the reader demodulated the impedance change, recovering transmitted data from the ASIC chip. The remote telemetry was formed with the ASIC chip, a receiver module, an AVR (Atmega-128), and data processing software written in Java.

Overall fabrication of the integrated smart contact lens

Because of the restriction to the ocular field of vision, a power receiver coil, a biosensor, and an f-DDS were fabricated on the peripheral area of a contact lens. The Cu power receiver coil was attached onto the ultrathin PET film (25 μm) with f-DDS using adhesive PDMS. The ASIC chip was implemented through the standard 0.18-μm CMOS process and diced into dimensions of 1.5 mm by 1.5 mm by 0.2 mm by chemical polishing and mechanical sawing. Afterward, the diced ASIC chip was attached, and WE, CE, and RE of the biosensor were deposited on the PET substrate. The power receiver coil, electrodes of the biosensor, and f-DDS were electrically connected with the ASIC chip using Au flip-chip bonding. For insulation and waterproofing, all devices on the PET substrate were coated with Parylene C and PDMS except for the sensing channel of the biosensor and the exposed electrodes of the f-DDS. Last, the integrated devices were molded into silicone hydrogels to fabricate a smart contact lens.

Preparation of diabetic retinopathy model rabbits

For in vivo glucose monitoring and diabetic retinopathy treatment, streptozotocin (STZ)–induced diabetic rabbit models were prepared by single injection of STZ (65 $mg \cdot kg^{-1}$) (1% STZ solution, diluted with 0.1 M citrate buffer, pH 4.4) to New Zealand white rabbits (2.0 kg) via the ear vein after fasting for 12 hours. After STZ injection, the rabbits with a plasma glucose concentration higher than 140 mg dl^{-1} were considered diabetic.

In vivo electrical detection of tear glucose levels

For in vivo real-time glucose monitoring, smart contact lenses were worn on each diabetic rabbit's eye, and the power transmitter coil was placed outside the eyes to transfer the wireless power to the receiver coil on the smart contact lens. The voltage was applied onto the glucose sensor in a pulsed manner, and the electrical measurement of glucose concentration was performed in real time with remote data transmission. Before 15 min of wireless tear glucose sensing, 2 U of insulin was injected to decrease the blood glucose level. After 5 min, ketamine was injected into diabetic rabbits for anesthetization. PBS was dropped onto the diabetic rabbit's eyes, and the smart contact lens was worn on the eye to start the wireless tear glucose monitoring.

Analysis of genistein penetration in vivo

The penetration of genistein released from smart contact lenses into eyes was investigated after positioning of the genistein-loaded smart contact lens onto rabbit eyes with wireless powering to operate the f-DDS. After 1 hour, the penetration of genistein was confirmed by fluorescence microscopic analysis in cryo-sectioned tissue of cornea, sclera, and retina using a fluorescence microscope (Fluoroskan Ascent, Thermo Fisher Scientific) at an excitation wavelength of 355 nm and an emission wavelength of 460 nm.

Electron microscopy and histological analysis

For the electron microscopic analysis of retinal blood vessels, the retinas were enucleated and fixed in 4 wt % glutaraldehyde and 1 wt %

osmium tetroxide solution. The samples were dehydrated with ethanol and sectioned to observe the cross section of retinal blood vessels by TEM (JEM-1010, JEOL). Histological analysis was performed with H&E staining of retinas fixed in 4% (w/v) paraformaldehyde for 24 hours.

In vivo treatment of diabetic retinopathy

The treatment of diabetic retinopathy using the smart contact lens was performed for 5 days on the right eyes of rabbits in five groups. The electrical power was wirelessly transmitted at a frequency of about 433 MHz using a power transmission coil to operate the f-DDS. As a control, an eye drop of PBS (0.05 ml, group 1), an eye drop of genistein (0.4 mM, 0.05 ml, group 2), and intravitreal injection of genistein (0.4 mM, 0.05 ml, group 3) were performed on the left eyes of each rabbit at the same time with the smart contact lens treatment. In addition, intravitreal injection of Avastin (0.05 ml, group 4) was performed on the left eye of rabbits. The right eyes of all groups were treated with smart contact lenses containing genistein (group 5).

Whole-mount retina immunofluorescence staining

The rabbit eyes were placed in 4% paraformaldehyde for 45 min. After fixation, retinas were dissected and flattened by applying curve-relieving cuts. The retinas were then fixed for an additional 1 hour. The retinas were washed twice with PBS and incubated with a 0.2% solution of Triton X-100 in PBS at room temperature for 1 hour. Last, vessels were stained with fluorescein isothiocyanate–labeled lectin from *Bandeiraea simplicifolia* (1:100, Sigma-Aldrich).

Immunostaining analysis

TUNEL assay was performed following the standard protocol. The immunostaining of collagen type IV and PECAM-1 was performed according to the manufacturer's protocols. The following antibodies were used: PECAM-1 antibody (sc-18916, Santa Cruz Biotechnology) and collagen type IV antibody (ab6586, Abcam). Nuclei were counterstained with 4′,6-diamidino-2-phenylindole. The images of vasculature were obtained at ×10 magnification. All fluorescence intensity was quantified by ImageJ program.

Study approval

All experiments were performed in accordance with the Association for Research in Vision and Ophthalmology Statement for the Use of Animals in Ophthalmic and Vision Research. The animal protocol was approved by the Institutional Animal Care and Use Committee at the College of Medicine, the Catholic University of Korea.

Statistical analysis

We performed one-sided statistical analyses using Student's *t* tests or one-way analysis of variance (ANOVA) with Bonferroni posttest. $P < 0.05$ was considered statistically notable. The quantification of fluorescence images was performed using ImageJ program. All data points were derived from three or more biological or technical replicates, as indicated for each experiment.

SUPPLEMENTARY MATERIALS

Supplementary material for this article is available at http://advances.sciencemag.org/cgi/content/full/6/17/eaba3252/DC1

View/request a protocol for this paper from *Bio-protocol*.

REFERENCES AND NOTES

1. B. Chu, W. Burnett, J. W. Chung, Z. Bao, Bring on the bodyNET. *Nature* **549**, 328–330 (2017).
2. T. Someya, Z. Bao, G. G. Malliaras, The rise of plastic bioelectronics. *Nature* **540**, 379–385 (2016).
3. J. Kim, A. S. Campbell, B. E.-F. de Ávila, J. Wang, Wearable biosensors for healthcare monitoring. *Nat. Biotechnol.* **37**, 389–406 (2019).
4. K. Yamagishi, I. Kirino, I. Takahashi, H. Amano, S. Takeoka, Y. Morimoto, T. Fujie, Tissue-adhesive wirelessly powered optoelectronic device for metronomic photodynamic cancer therapy. *Nat. Biomed. Eng.* **3**, 27–36 (2019).
5. H. Lee, T. K. Choi, Y. B. Lee, H. R. Cho, R. Ghaffari, L. Wang, H. J. Choi, T. D. Chung, N. Lu, T. Hyeon, S. H. Choi, D.-H. Kim, A graphene-based electrochemical device with thermoresponsive microneedles for diabetes monitoring and therapy. *Nat. Nanotechnol.* **11**, 566–572 (2016).
6. J. H. Koo, S. Jeong, H. J. Shim, D. Son, J. Kim, D. C. Kim, S. Choi, J.-I. Hong, D.-H. Kim, Wearable electrocardiogram monitor using carbon nanotube electronics and color-tunable organic light-emitting diodes. *ACS Nano* **11**, 10032–10041 (2017).
7. M. M. Dua, A. Navalgund, S. Axelrod, L. Axelrod, P. J. Worth, J. A. Norton, G. A. Poultsides, G. Triadafilopoulos, B. C. Visser, Monitoring of gastric myoelectric activity after pancreaticoduodenectomy. *Am. J. Physiol. Gastrointest. Liver Physiol.* **315**, G743–G751 (2018).
8. H. Lee, E. Kim, Y. Lee, H. Kim, J. Lee, M. Kim, H.-J. Yoo, S. Yoo, Toward all-day wearable health monitoring: An ultralow-power, reflective organic pulse oximetry sensing patch. *Sci. Adv.* **4**, eaas9530 (2018).
9. J. H. Prescott, S. Lipka, S. Baldwin, N. F. Sheppard Jr., J. M. Maloney, J. Coppeta, B. Yomtov, M. A. Staples, J. T. Santini Jr., Chronic, programmed polypeptide delivery from an implanted, multireservoir microchip device. *Nat. Biotechnol.* **24**, 437–438 (2006).
10. B. P. Timko, T. Dvir, D. S. Kohane, Remotely triggerable drug delivery systems. *Adv. Mater.* **22**, 4925–4943 (2010).
11. D. Son, J. Lee, S. Qiao, R. Ghaffari, J. Kim, J. E. Lee, C. Song, S. J. Kim, D. J. Lee, S. W. Jun, S. Yang, M. Park, J. Shin, K. Do, M. Lee, K. Kang, C. S. Hwang, N. Lu, T. Hyeon, D.-H. Kim, Multifunctional wearable devices for diagnosis and therapy of movement disorders. *Nat. Nanotechnol.* **9**, 397–404 (2014).
12. D.-H. Kim, N. Lu, R. Ghaffari, Y.-S. Kim, S. P. Lee, L. Xu, J. Wu, R.-H. Kim, J. Song, Z. Liu, J. Viventi, B. de Graff, B. Elolampi, M. Mansour, M. J. Slepian, S. Hwang, J. D. Moss, S.-M. Won, Y. Huang, B. Litt, J. A. Rogers, Materials for multifunctional balloon catheters with capabilities in cardiac electrophysiological mapping and ablation therapy. *Nat. Mater.* **10**, 316–323 (2011).
13. R. Farra, N. F. Sheppard Jr., L. McCabe, R. M. Neer, J. M. Anderson, J. T. Santini Jr., M. J. Cima, R. Langer, First-in-human testing of a wirelessly controlled drug delivery microchip. *Sci. Transl. Med.* **4**, 122ra21 (2012).
14. K. Mansouri, F. A. Medeiros, A. Tafreshi, R. N. Weinreb, Continuous 24-hour intraocular pressure monitoring with a contact lens sensor: Safety, tolerability, and reproducibility in glaucoma patients. *Arch. Ophthalmol.* **130**, 1534–1539 (2012).
15. N. M. Farandos, A. K. Yetisen, M. J. Monteiro, C. R. Lowe, S. H. Yun, Contact lens sensors in ocular diagnostics. *Adv. Healthc. Mater.* **4**, 792–810 (2015).
16. E. Elhawy, G. Kamthan, C. Q. Dong, J. Danias, Pseudoexfoliation syndrome, a systemic disorder with ocular manifestations. *Hum. Genomics* **6**, 22–31 (2012).
17. J. Kim, M. Kim, M.-S. Lee, K. Kim, S. Ji, Y.-T. Kim, J. Park, K. Na, K.-H. Bae, H. K. Kim, F. Bien, C. Y. Lee, J.-U. Park, Wearable smart sensor systems integrated on soft contact lenses for wireless ocular diagnostics. *Nat. Commun.* **8**, 14997 (2017).
18. J. Park, J.-H. Kim, S.-Y. Kim, W. H. Cheong, J. Jang, Y.-G. Park, K. Na, Y.-T. Kim, J. H. Heo, C. Y. Lee, J. H. Lee, F. Bien, J.-U. Park, Soft, smart contact lenses with integrations of wireless circuits, glucose sensors, and displays. *Sci. Adv.* **4**, eaap9841 (2018).
19. J. T. Baca, D. N. Finegold, S. A. Asher, Tear glucose analysis for the noninvasive detection and monitoring of diabetes mellitus. *Ocul. Surf.* **5**, 280–293 (2007).
20. H. Yao, A. J. Shum, M. Cowan, I. Lähdesmäki, B. A. Parviz, A contact lens with embedded sensor for monitoring tear glucose level. *Biosens. Bioelectron.* **26**, 3290–3296 (2011).
21. X. Xiao, T. Siepenkoetter, P. Ó. Conghaile, D. Leech, E. Magner, Nanoporous gold-based biofuel cells on contact lenses. *ACS Appl. Mater. Interf.* **10**, 7107–7116 (2018).
22. Y.-T. Liao, H. Yao, A. Lingley, B. A. Parviz, B. P. Otis, A 3-μW CMOS glucose sensor for wireless contact-lens tear glucose monitoring. *IEEE J. Solid-State Circuits* **47**, 335–344 (2012).
23. E. J. Oh, J.-S. Choi, H. Kim, C.-K. Joo, S. K. Hahn, Anti-Flt1 peptide-hyaluronate conjugate for the treatment of retinal neovascularization and diabetic retinopathy. *Biomaterials* **32**, 3115–3123 (2011).
24. W. Gao, S. Emaminejad, H. Y. Y. Nyein, S. Challa, K. Chen, A. Peck, H. M. Fahad, H. Ota, H. Shiraki, D. Kiriya, D.-H. Lien, G. A. Brooks, R. W. Davis, A. Javey, Fully integrated wearable sensor arrays for multiplexed *in situ* perspiration analysis. *Nature* **529**, 509–514 (2016).

25. H. Lee, C. Song, Y. S. Hong, M. S. Kim, H. R. Cho, T. Kang, K. Shin, S. H. Choi, T. Hyeon, D.-H. Kim, Wearable/disposable sweat-based glucose monitoring device with multistage transdermal drug delivery module. *Sci. Adv.* **3**, e1601314 (2017).
26. Y. J. Hong, H. Lee, J. Kim, M. Lee, H. J. Choi, T. Hyeon, D.-H. Kim, Multifunctional wearable system that integrates sweat-based sensing and vital-sign monitoring to estimate pre–/post-exercise glucose levels. *Adv. Funct. Mater.* **28**, 1805754 (2018).
27. E. J. Kappert, D. Pavlenko, J. Malzbender, A. Nijmeijer, N. E. Benes, P. A. Tsai, Formation and prevention of fractures in sol-gel derived thin films. *Soft Matter* **11**, 882–888 (2015).
28. F.-L. Wong, A. Abdul-Aziz, Comparative study of poly(vinyl alcohol)-based support materials for the immobilization of glucose oxidase. *J. Chem. Technol. Bioechnol.* **83**, 41–46 (2008).
29. S. Vaddiraju, H. Singh, D. J. Burgess, F. C. Jain, F. Papadimitrakopoulos, Enhanced glucose sensor linearity using poly(vinyl alcohol) hydrogels. *J. Diabetes Sci. Technol.* **3**, 863–874 (2009).
30. D. Liu, Q. Wu, Y. Zhu, Y. Liu, X. Xie, S. Li, H. Lin, W. Chen, F. Zhy, Co-delivery of metformin and levofloxacin hydrchloride using biodegradable thermosensitive hydrogel for the treatment of corneal neovascularization. *Drug Deliv.* **26**, 522–531 (2019).
31. L. M. Berstein, Metformin: Not only per os. *Expert Rev. Endocrinol. Metab.* **13**, 63–65 (2018).
32. J. Kim, A. Conway, A. Chauhan, Extended delivery of ophthalmic drugs by silicone hydrogel contact lenses. *Biomaterials* **29**, 2259–2269 (2008).
33. H. Son, H. Cho, J. Koo, Y. Ji, B. Kim, H.-J. Park, J.-Y. Sim, A low-power wide dynamic-range current readout circuit for ion-sensitive FET sensors. *IEEE Trans. Biomed. Circuits Syst.* **11**, 523–533 (2017).

Acknowledgments

Funding: This work was financially supported by Samsung Science & Technology Foundation (SRFC-IT1401-03) in Korea. This research was supported by the Center for Advanced Soft-Electronics (Global Frontier Project, CASE-2015M3A6A5072945) and the Basic Science Research Program (2017R1E1A1A03070458 and 2020R1A2C3014070) of the National Research Foundation (NRF) funded by the Ministry of Science and ICT, Korea. This work was also supported by the World Class 300 Project (S2482887) of the Small and Medium Business Administration (SMBA), Korea. D.M. was supported by the National Eye Institute (K08EY028176 and P30-EY026877) and the Research to Prevent Blindness Foundation. **Author contributions:** S.K.H. conceived and supervised the project, designed experiments, interpreted data, and wrote the manuscript. D.H.K. and S.-K.K. performed experiments, collected samples, analyzed and interpreted data, and wrote the manuscript. J.K., C.J., B.H.M., K.J.L., E.K., and S.H.Y. contributed to preparing and designing the smart contact lens. G.-H.L., S.S., J.-Y.S., and Z.B. contributed to designing and performing the electrical experiments. J.W.M. and C.J. contributed to designing and performing the animal experiments. D.M. contributed to analyzing and interpreting the data and revising the manuscript. All authors contributed to critical reading and revision of this manuscript. **Competing interests:** S.H.Y., E.K., K.J.L., D.H.K., C.-K.J., and S.K.H. are inventors on a patent related to this work filed by Harvard Medical School and PHI Biomed Co. (no. US 2016/0223842A1, filed 4 August 2016). K.J.L., B.H.M., D.H.K., and S.K.H. are inventors of a patent related to this work filed by POSTECH and PHI Biomed Co. [no. US 10,399,291B2, filed 3 September 2019, registered in the United States and Korea (10-2016-0050139), and applied in Japan (2018-507476) and Europe (16783461.3)]. The authors declare that they have no other competing interests. **Data and materials availability:** All data needed to evaluate the conclusions in the paper are present in the paper and/or the Supplementary Materials. Additional data related to this paper may be requested from the authors.

Submitted 23 November 2019
Accepted 31 January 2020
Published 24 April 2020
10.1126/sciadv.aba3252

Citation: D. H. Keum, S.-K. Kim, J. Koo, G.-H. Lee, C. Jeon, J. W. Mok, B. H. Mun, K. J. Lee, E. Kamrani, C.-K. Joo, S. Shin, J.-Y. Sim, D. Myung, S. H. Yun, Z. Bao, S. K. Hahn, Wireless smart contact lens for diabetic diagnosis and therapy. *Sci. Adv.* **6**, eaba3252 (2020).

Wireless smart contact lens for diabetic diagnosis and therapy

Do Hee Keum, Su-Kyoung Kim, Jahyun Koo, Geon-Hui Lee, Cheonhoo Jeon, Jee Won Mok, Beom Ho Mun, Keon Jae Lee, Ehsan Kamrani, Choun-Ki Joo, Sangbaie Shin, Jae-Yoon Sim, David Myung, Seok Hyun Yun, Zhenan Bao and Sei Kwang Hahn

Sci Adv **6** (17), eaba3252.
DOI: 10.1126/sciadv.aba3252